IEEE Access
Multidisciplinary | Rapid Review | Open Access Journal

Received March 26, 2022, accepted May 21, 2022, date of publication May 26, 2022, date of current version June 1, 2022.

Digital Object Identifier 10.1109/ACCESS.2022.3178124

Simulation Research on the Forward Problem of Magneto-Acoustic Concentration Tomography of Magnetic Nanoparticles With Magnetic Induction Based on the Relaxation Time of Magnetic Nanoparticles

XIAOHENG YAN, DI SUN, ZHENGXING LI, AND WEIHUA CHEN
Faculty of Electrical and Control Engineering, Liaoning Technical University, Huludao, Liaoning 125105, China

Corresponding author: Di Sun (17742937355@163.com)

This work was supported in part by the Natural Science Foundation of Liaoning Province under Grant 2019ZD0039, and in part by the Basic Research Project Foundation from Liaoning Education Department under Grant LJ2020JCL003.

ABSTRACT Magneto-acoustic concentration tomography of magnetic nanoparticles (MNPs) with magnetic induction (MACT-MI) is an emerging method for magnetic particle imaging based on the magneto-acoustic coupling effect. However, the limitation of this method is that the concentration of magnetic nanoparticles in the human body should be regulated to prevent excessive metabolic pressure on the kidneys. Therefore, on the premise of keeping the concentration constant, the magnetic calculation method of MNPs under the relaxation mechanism is specifically studied. We deduce the optimal particle size for imaging and greatly increased the magnetic force and sound pressure of MACT-MI, which is more conducive to the acquisition of magneto-acoustic signals. In addition, rationally increasing the fluid ambient temperature and selecting the diameter of magnetic nanoparticles according to different target tissue fluids can also optimize the imaging effect. This research provides a technical basis for the application of MNPs in tumor markers and targeted drug release.

INDEX TERMS Magneto-acoustic concentration tomography of magnetic nanoparticles with magnetic induction (MACT-MI), magnetic nanoparticles (MNPs), relaxation, optimal particle size.

I. INTRODUCTION

In recent years, magnetic nanoparticles (MNPs) have increasingly become an efficient medium in modern medical imaging and therapy due to their superior magnetic guidance and biocompatibility and have been successfully applied in various fields of biomedicine. In 2007, Norton discovered that introducing magnetic nanoparticles into the body could be used as an antibody marker for targeting tumor cells or as a cardiovascular contrast agent [1]. In 2012, Hu *et al.* proposed a new imaging technology fused with superparamagnetic nanoparticles and obtained clear tissue boundary images, which demonstrated the feasibility of MNP imaging [2]. In 2016, Mariappan implanted superparamagnetic iron oxide nanoparticles into mice and used MAT-MI to successfully detect and reconstruct the distribution of superparamagnetic iron oxide nanoparticles[3]. In 2020, our team proposed magneto-acoustic magnetic particle concentration imaging, which uses MNPs to mark target biological tissues. Under the excitation of a high-intensity pulsed magnetic field, MNPs vibrate to generate magneto-acoustic signals. The use of ultrasonic transducers to collect the magneto-acoustic signals can assist the image reconstruction of nanoparticle concentration [4], [5]. In 2020, Xu Zhengyang studied the inverse problem of MACT-MI based on the method of moments and improved the quality of image reconstruction by optimizing the image reconstruction algorithm through total variation regularization [6]. In 2021, Li Zhengxing added permanent magnets of the same polarity to the original MACT-MI imaging device so that the MNPs could receive a stronger magnetic force and excite magneto-acoustic signals with a larger signal-to-noise ratio [7]. The abovementioned research

The associate editor coordinating the review of this manuscript and approving it for publication was Carmelo Militello.

has promoted the development of MAT-MI toward higher resolution and better imaging effects. However, the current studies of MAT-MI in our group are all based on the premise of neglecting the relaxation effect of MNPs.

At present, there are many medical methods that use MNPs for imaging and treatment, such as magnetic particle imaging [8], [9], magnetic particle thermo-acoustic imaging [10], [11], and magnetic nano-hyperthermia [12], [13]. In 2002, E. Romanus considered the orientation relaxation of MNPs under the action of an alternating magnetic field and derived the analytical relationship and calculation method of energy loss in fluid media [14]. In the same year, the team demonstrated that magnetic relaxation measurement can be used as a new technique to detect the number and location of MNPs through in vivo experiments in mice [15]. In 2008, J. Fortin placed MNPs into tumor cells and predicted the intracellular heating efficiency of iron oxide nanoparticles using a relaxation mechanism [16]. In 2010, Hergt used the Néel relaxation model to derive the optimal diameter of MNPs for tumor hyperthermia [17]. In 2015, Yoon measured the magnetic properties and size distribution of Fe_3O_4 at room temperature using a superconducting quantum interference device (SQUID) and demonstrated that the size and shape of MNPs directly affect their magnetic properties [18]. In the same year, Perreard used the Brown relaxation time of MNPs to measure the temperature of their surrounding micro-environment [19]. In 2021, Guo Gepu proposed a new MAT-MI harmonic imaging method considering the relaxation time of MNPs based on the magneto-acoustic second harmonic generated by MNPs vibrating under an alternating magnetic field [20]. On the basis of the above studies, the effect of the relaxation mechanism on MNP imaging cannot be ignored.

Most previous MACT-MI studies have improved the excitation device and optimized the imaging algorithm. However, research on the dynamic magnetization process of MNPs in fluid media has also improved the imaging effect. To improve the imaging quality of MACT-MI, it is necessary to increase the concentration of magnetic nanoparticles to a certain extent. However, if the concentration is too high, the renal metabolism of magnetic nanoparticles is poor, which is detrimental to human health. Therefore, by means of the relaxation mechanism, according to the actual clinical temperature and target tissue fluid, the particle size of the magnetic nanoparticles can be optimized to enhance the intensity of the magneto-acoustic signal without excessive particle concentration. In this paper, on the premise of maintaining an unchanged concentration of magnetic nanoparticles, a calculation method for the magnetic force under the relaxation mechanism is deduced, and then the magnetic force and sound pressure of different particle sizes, different tissue fluids and different temperatures are calculated by establishing a biological tissue model embedded with magnetic nanoparticle clusters. This study shows that the imaging quality of MACT-MI can be significantly improved by optimizing the magnetic nanoparticles at the optimal particle size. At the same time, this study provides new research ideas for more targeted optimization of the clinical application conditions of MACT-MI (such as supplemented by heating methods) according to different target tissues.

II. THEORETICAL ANALYSIS

A. PRINCIPLE OF TOMOGRAPHY

As shown in Figure 1, a microsecond pulse current is passed through a coil, and the resulting alternating magnetic field is applied to the target tissue marked by MNPs. MNPs vibrate under electromagnetic force and generate sound waves. The sound pressure signal inside the biological tissue is collected by the ultrasonic transducer, and the shape and position information of the target tissue is inverted via sound pressure wave equation.

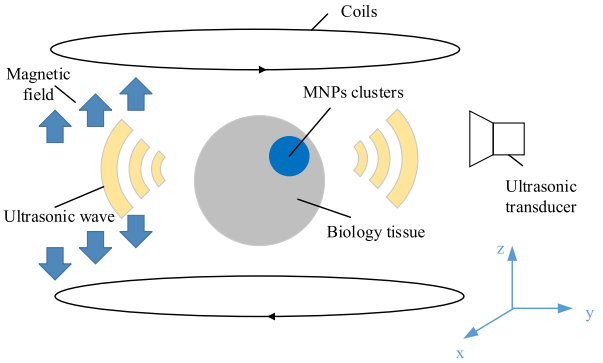

FIGURE 1. Schematic diagram of MACT-MI.

B. MAGNETIZATION AND RELAXATION OF MNPS

When there is no external magnetic field, the MNPs are randomly distributed. The total magnetic moment m is zero macroscopically and without external magnetism. When MNPs are placed in an alternating magnetic field, their magnetic moments can be expressed as

$$\boldsymbol{m} = Vf_m\boldsymbol{M} \tag{1}$$

where V is the volume of a single magnetic nanoparticle and f_{m} is the volume fraction of the magnet material in the nanoparticle. The product of the two values is the volume of the magnetic material in the nanoparticle. The magnetic susceptibility of MNPs and biological fluid media are χ_{np} and χ_{medium}, respectively. Compared with the magnetic susceptibility values in MNPs, the magnetic susceptibility of fluid media (biological tissues) can be ignored [21]. When an alternating magnetic field $\boldsymbol{H}$ is applied to the biological tissue embedded in MNPs, the magnetization $\boldsymbol{M}$ can be described as

$$\boldsymbol{M} = \left(\chi_{np} - \chi_{medium}\right)\boldsymbol{H} = \chi_{np}\frac{\boldsymbol{B}}{\mu_0} \tag{2}$$

In the formula above, the magnetic susceptibility χ_{np} of MNPs is

$$\chi_{np} = \frac{\chi_0}{1 + i\omega\tau} \tag{3}$$

where χ_0 is the equilibrium magnetic susceptibility, $\chi_0 = \mu_0 \boldsymbol{M}_S^2 V / (3k_B T)$. k_B is the Boltzmann constant and $\boldsymbol{M}_S$ is the saturation magnetization intensity. ω is the angular frequency of the excitation current, and τ is the effective relaxation time of the MNPs. The complex form of magnetic susceptibility is written as

$$\chi' = \frac{\chi_0}{1 + (\omega\tau)^2} \tag{4a}$$

$$\chi'' = \frac{\omega\tau}{1 + (\omega\tau)^2}\chi_0 \tag{4b}$$

However, only the energy generated by the imaginary part of the magnetic susceptibility is retained in the magnetic field energy calculation, so it is sufficient just considering the imaginary part of the magnetization rate in the calculation of the magnetic force and sound pressure [12]. Equation (3) shows that the magnetic susceptibility of MNPs is affected by the relaxation of MNPs in a fluid environment.

Whether the relaxation process can be ignored during magnetization of magnetic nanoparticles is decided by the two following factors:

The frequency of the excitation magnetic field. Whether the relaxation effect must be considered depends largely on the frequency f of the applied magnetic field. If the change rate of the magnetic field is small enough to satisfy the relationship $\boldsymbol{f} \ll 1/\tau$, magnetization of magnetic particles can follow the change of magnetic field and the relaxation effect can be ignored. Under this condition the magnetization process of particles can be described by Langevin function. If the magnetic field frequency changes too fast, hysteresis effect will occur and the magnetization of particles will become complicated. When the frequency further increases, the particle cannot keep up with the change of magnetic field to adjust the direction of magnetic moment, and its magnetization will sharply decrease. Thus, the relaxation effect cannot be ignored and dominates the magnetization process. The higher the excitation frequency, the greater the relaxation effect on the magnetization response of magnetic nanoparticles. In this study, the applied frequency is at MHz level, and the calculated relaxation time is about microseconds. So, the relaxation process in this study cannot be ignored.

Temperature: When the temperature reaches Curie temperature, the magnetic moment of neatly arranged magnetic domain is destroyed and disintegrated and the average magnetic moment becomes zero. At this moment ferromagnetic material becomes paramagnetic material, and the permeability of corresponding ferromagnetic material is transformed into that of paramagnetic material. So, the relaxation process can be ignored. However, the Curie point of different ferromagnetic materials differs due to the difference of materials. The Curie point of some ferromagnetic materials can reach more than 360T, which is far higher than the safe temperature range of human body. The relaxation process cannot be ignored under this temperature range.

Néel relaxation is an orientation rotation of the magnetic nucleus along the magnetic field direction by magnetic field forces. However, Brown relaxation is the random movement of magnetic particles that hinders the rotation and alignment of the magnetic moment. The two relaxations influence each other and restrict each other to achieve dynamic equilibrium [22]. The effective relaxation time determined by both Brown relaxation time and Néel relaxation time is

$$\tau = \frac{\tau_B \tau_N}{\tau_B + \tau_N} \tag{5}$$

The Brown relaxation time is

$$\tau_B = \frac{3\eta V}{KT} \tag{6}$$

The Néel relaxation time is

$$\tau_N = \tau_0 \exp\left(KV/k_B T\right) \tag{7}$$

where η is the viscosity coefficient of the fluid medium; T is the temperature and K is the anisotropy constant. k_B is the Boltzmann constant and τ_0 is usually 10^{-9}~10^{-10}. In a fluid environment, the relaxation of MNPs is not only related to the particle sizes but also depends on the viscosity of the environmental medium. In addition, the relaxation of MNPs is also related to the excitation frequency. If the excitation frequency is too high, the relaxation of MNPs cannot follow the change of the magnetic field, and the magnetization of MNPs is limited. Therefore, the frequencies currently studied are mostly MHz and below.

When MNPs are exposed to an alternating magnetic field $\boldsymbol{B}$, the magnetic field energy U of a single particle is [4]

$$U = \frac{1}{2}\boldsymbol{m} \cdot \tilde{\boldsymbol{B}} = -\frac{\chi_{np} V f_m}{2\mu_0}\tilde{\boldsymbol{B}}^2 \tag{8}$$

Introducing the time term $s(t)$, the magnetic flux density is denoted as $\widetilde{\boldsymbol{B}} = \boldsymbol{B}s(t)$. Then, the electromagnetic force can be calculated according to the principle of virtual work. Considering the magnetic field in the z direction only, the magnetic force can be expressed as

$$F_m = -N\frac{\chi_{np} V f_m}{\mu_0} B_Z \frac{\partial B_Z}{\partial z} s^2(t) \tag{9}$$

where N is the number of magnetic nanoparticles. In any particle clusters, although the particle sizes cannot be single and uniform, the distribution still follows a certain pattern. The magnetic force and sound pressure of multi-sized MNPs are obtained by weighting and integrating the particle size distribution probability of MNPs [17]. Assume that the particle size distribution of the multi-sized particles follows a normal distribution function [23] as

$$g(\mathrm{D}) = \frac{1}{\sqrt{2\pi}\sigma}\exp\left[\frac{-(\ln \mathrm{D}/\mathrm{D}_0)^2}{2\sigma^2}\right] \tag{10a}$$

$$\int_0^\infty g(\mathrm{D})d\mathrm{D} = 1 \tag{10b}$$

where D_0 is the mean particle diameter and the MNPs are spherical. σ is the standard deviation of the particle size distribution. Substitute $V = 4\pi(\mathrm{D}/2)^3/3$. Therefore, the average

magnetic force of multi-sized MNPs can be expressed as

$$\overline{F_{\mathrm{m}}} = -\int_0^{\infty} \frac{4}{3}\pi g\,(\mathrm{D})\left(\frac{\mathrm{D}}{2}\right)^3 N\frac{\chi_{np} f_m}{\mu_0} B_Z \frac{\partial B_Z}{\partial z} d\mathrm{D} \quad (11)$$

C. SOUND PRESSURE WAVE EQUATION

Magnetic force stimulates the displacement and small amplitude vibration of MNPs in the fluid medium and then generates an ultrasonic signal that propagates outwards. For a medium with a constant density, the wave equation of sound pressure is

$$\nabla^2 p\,(r,t) - \frac{1}{c_s^2}\cdot\frac{\partial^2 p\,(r,t)}{\partial t^2} = \nabla\cdot F_{\mathrm{m}} \quad (12)$$

The boundary condition of the sound field in MACT-MI is free, which means the sound pressure decays to zero at infinity. Meanwhile, the following initial conditions are introduced:

$$\begin{cases} p|_{t=0^-} = 0 \\ \left.\dfrac{\partial p}{\partial t}\right|_{t=0^-} = 0 \end{cases} \quad (13)$$

where $p\,(\boldsymbol{r},t)$ is the sound pressure field; r is the source location, and c_{s} is the ultrasound propagation velocity in the biological tissue. The sound pressure [24] is calculated by Green's function $G\left(\boldsymbol{r'},\boldsymbol{r},t\right) = \frac{\delta(t-|\boldsymbol{r'}-\boldsymbol{r}|/c_s)}{|\boldsymbol{r'}-\boldsymbol{r}|}$. The sound field analytical solution is

$$p\left(\boldsymbol{r'},t\right) = -\frac{1}{4\pi}\iiint_{\Omega} d^3\boldsymbol{r}\nabla_{\boldsymbol{r}}\cdot F_{\mathrm{m}}\left(\boldsymbol{r},t\right) G\left(\boldsymbol{r'},\boldsymbol{r},t\right) \quad (14)$$

where $\boldsymbol{r'}$ is the position of the detection point and $\nabla_{\boldsymbol{r}}$ is the relative source space derivative.

D. NUMERICAL SIMULATION

In this paper, COMSOL Multi-physics is used to establish a three-dimensional biological tissue model embedded with MNPs and conduct electromagnetic-acoustic multi-coupling analysis. A sphere with a diameter of 10 mm is used to simulate the MNP cluster model. Another sphere with a diameter of 60 mm is used to simulate normal biological tissues, and the two spheres are placed in the magnetic field generated by a single-turn Maxwell coil with a radius of 60 mm. The model is shown in Figure 2. Since the Maxwell coil has a zero magnetic field zone in its central area, the center of the MNP cluster is shifted to (0,5,20).

The magnetic field intensity $\boldsymbol{B}_z$ on the axis connecting the centers of the two coils is

$$\boldsymbol{B}_z = \frac{\mu nIR^2}{\sqrt{\left(R^2+(Z+\frac{\sqrt{3}}{2}R)^2\right)^3}} - \frac{\mu nIR^2}{\sqrt{\left(R^2+(Z-\frac{\sqrt{3}}{2}R)^2\right)^3}} \quad (15)$$

where R is the radius of the Maxwell coil. The narrow pulse excitation currents I in opposite directions are passed through the two coils, and their expression is

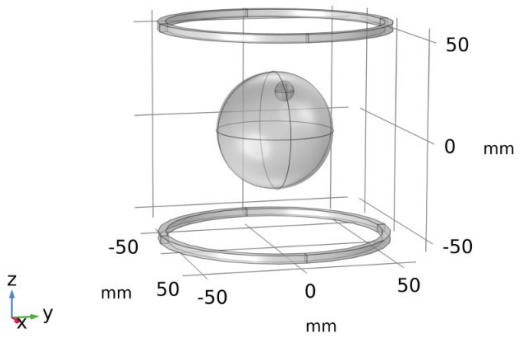

FIGURE 2. Biological tissue and MNP cluster model.

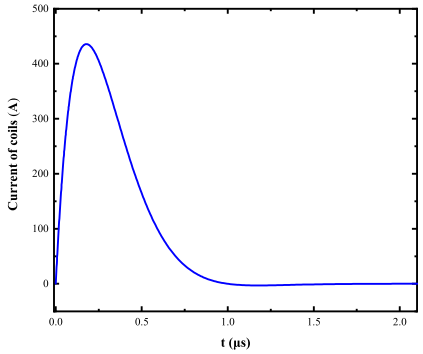

FIGURE 3. Current excitation curve.

$I(t) = 2\times10^3\times \mathrm{e}^{-5\times10^6\mathrm{t}}\times\sin(2\pi\times10^6\mathrm{t})$. The current waveform is shown in Figure 3.

Inside the MNP cluster model are water-soluble ferrofluid superparamagnetic nanoparticles. Taking an aqueous solution of EMG 308 (Ferrotec, NH, USA) as an example, the IONP (iron oxide nanoparticle) concentration is 4 mg Fe/ml. The magnetic core is Fe_2O_3, and the particle size range is 5–20 nm. The average particle size is 15 nm [3].

Usually, the solution is injected into human body through intravenous injection, and MNPs enter the target biological tissue fluid through the blood after staying in the vascular system for a period of time. It is preliminarily assumed that MNPs are particles with uniform particle size, and the fluid environment is human blood. The concentration is constant during this process. The parameters of the MNPs and the fluid environment are shown in Table 1. In this MNP Cluster model shown in Figure 4 and parameters, the magnetic force and sound pressure of MACT-MI are simulated and studied.

III. RESULTS

A. MACT-MI MAGNETIC ANALYSIS

After setting the initial parameters, Eq. (11) was used to calculate the magnetic force of the biological model exposed to the Maxwell coils. The magnetic force magnitude distribution on the YOZ plane is shown in Figure 5. The magnetic force inside and outside the MNP cluster is significantly different because the magnetic susceptibility of the MNPs is greater

TABLE 1. The initial parameters of the simulation.

Expressions	Parameters	Values
D	Nominal particle diameter	15 nm
$V = \pi D^3 / 6$	Particle volume	
T	Temperature	310 K
k_B	Boltzmann constant	1.3806×10^{-23} J/K
K	anisotropy constant	1.6×10^4 J/m^3
η	Viscosity coefficient (blood)	3.65×10^{-3} Pa.s
N	Number concentration	2.15×10^{19}/ml

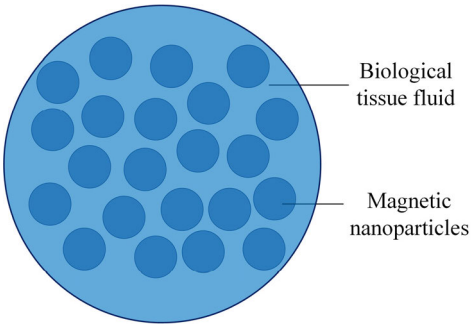

FIGURE 4. MNP cluster model.

than that of biological fluid media. In addition, since the magnetic field near the Maxwell coil is stronger, the magnetic force is also more obvious. To observe the magnetic force of the MNPs, the center M (0,5,20) of the MNP cluster model was selected as the observation point. The waveform of the magnetic force magnitude at this point with time is shown in Figure 6.

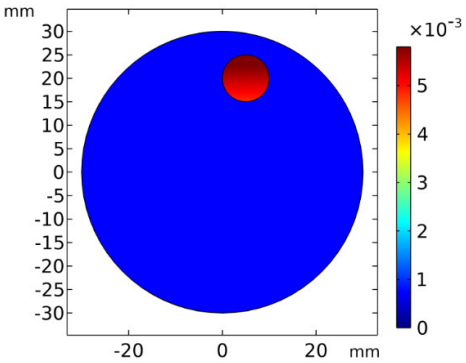

FIGURE 5. Magnetic force magnitude distribution.

1) EFFECT OF FLUID MEDIUM ON MAGNETIC FORCE

The temperature and viscosity of the fluid environment to which MNPs are exposed affect the relaxation process, so the magnetic force varies with different temperatures and different biological tissue fluids. The viscosity coefficients of different tissue fluids of the human body are shown in Table 2. Based on this data, this article calculates the magnetic force at

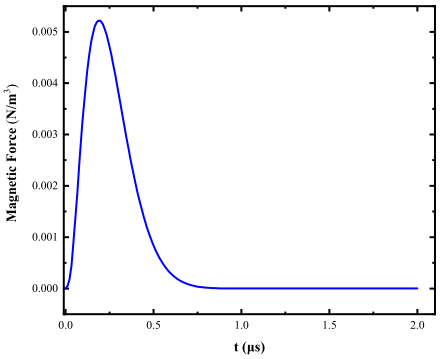

FIGURE 6. Magnetic force curve.

the cluster center M(0,5,20) within the tolerable temperature range under the premise of ensuring the safety of the human body [17].

TABLE 2. Viscosity parameters of different tissue fluids in the human body.

Biological tissue fluid	Coefficient of viscosity
Water	6.40×10^{-4} Pa.s
Cerebrospinal Fluid	7.84×10^{-4} Pa.s
Lymphatic Fluid	1.80×10^{-3} Pa.s
Blood	3.65×10^{-3} Pa.s

In the process of exploring the influence of the fluid medium environment on the magnetic force, it is found that when the diameter D of the single-size MNPs is 15 nm, as shown in Figure 7, the magnetic force gradually increases with warming. When the temperature remains constant, the magnetic force decreases as the viscosity of the fluid medium increases. Therefore, increasing the temperature reasonably and reducing the viscosity of the fluid medium can obtain a more significant magneto-acoustic signal. When D = 10 nm, as shown in Figure 8, the magnetic force gap between different viscosity coefficients is small at the same temperature, and the temperature is inversely proportional to the magnetic force. This is because the equilibrium susceptibility $\chi_0 = \mu_0 \boldsymbol{M}_S^2 V / (3k_B T)$ is more affected by temperature than the diameter. However, in any case, the magnetic force changes slightly compared to D = 15 nm.

2) EFFECT OF MNP PARTICLE SIZE ON MAGNETIC FORCE

From the above study, it is clear that both the temperature and viscosity of the fluid medium affect the magnetic force with different particle sizes. Therefore, the relationship between particle size and magnetic force was further explored under the condition of strict control of variables.

Figure 9 shows the magnetic force variation of MNPs with diameter and temperature. The fluid medium is blood, and the viscosity is 3.65×10^{-3} Pa.s. As the particle size expands, the magnetic force increases first and then decreases. This result

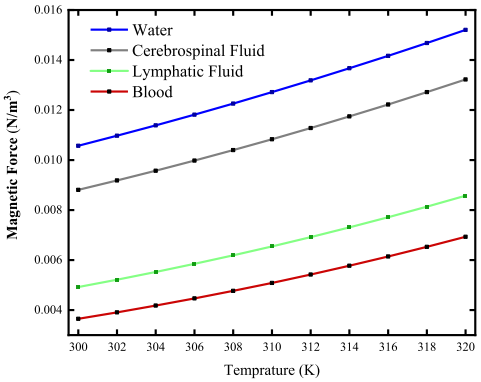

FIGURE 7. D = 15 nm variation of magnetic force with temperature and viscosity.

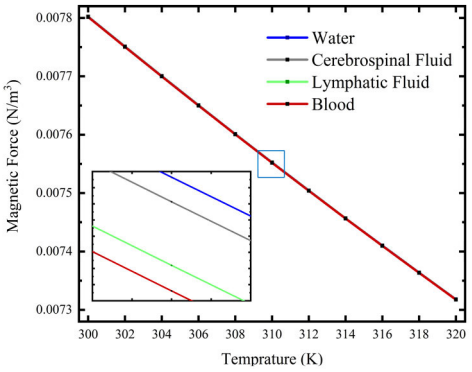

FIGURE 8. D = 10 nm variation of magnetic force with temperature and viscosity.

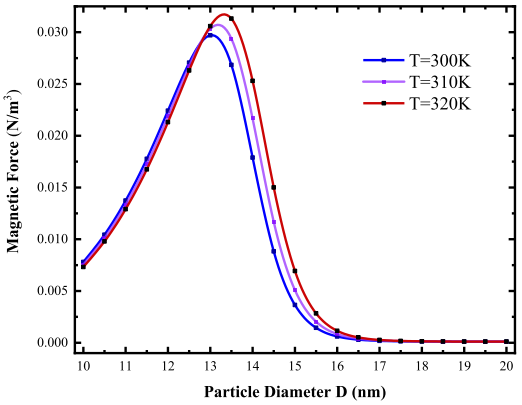

FIGURE 9. $\eta = 3.65 \times 10^{-3}$, variation in magnetic force with diameter and temperature.

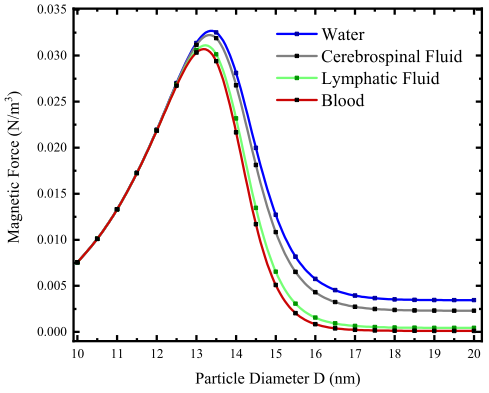

FIGURE 10. T = 310 K variation of magnetic force with diameter and viscosity.

demonstrates that the magnetic force reaches a maximum when the diameter D is approximately 13.5 nm at the same temperature, which indicates that an optimal particle size exists in MACT-MI. In addition, in the range of particle sizes shorter than 13.5 nm, the magnetic force gap between different temperatures is not obvious. When the particle sizes are larger than 13.5 nm, raising the temperature has a positive effect on the magnetic force to some extent, but compared with the adjustment of the particle size, this approach is much inferior.

Figure 10 shows the trend of the magnetic force of MNPs with changes in diameter and viscosity. The temperature was set to the normal body temperature T = 310 K. Similar to the last study, the peak of magnetic force appears again near D = 13.5 nm. This again affirms the inference that D = 13.5 nm is the optimal particle size of this MACT-MI system to excite the maximum magnetic force under the present simulation conditions. When D < 13.5 nm, the magnetic force difference generated by different media viscosities is too small and can even be ignored. When D > 13.5 nm, the increase in the viscosity of the fluid medium gradually affects or even weakens the magnetic force of the MNPs. This result is consistent with the previously described phenomenon that the effect of viscosity on the magnetic force is different for D = 10 nm and D = 15 nm.

From the above analysis, it can be seen that the particle sizes of MNPs have a crucial influence on the magnetic force. From Equation (15), it can be seen that the magnetic force is proportional to both the particle volume and the magnetic susceptibility, but the relationship between the two and the particle size is contrary: Increasing the particle size can expand the volume of MNPs but also prolong the effective relaxation time and thus reduce the magnetic susceptibility to some extent. Therefore, the optimal particle size to excite the maximum magnetic force is the result of the combined contribution of MNP volumes and effective relaxation times.

Generally, the effective relaxation time is dominated by the faster of the two relaxation mechanisms, as shown in Figure 11. From Equation (6) and Equation (7), the dependence of the two relaxations on particle size is quite different. Taking $\tau_N = \tau_B$ as the boundary, the effective relaxation time is dominated by the Néel relaxation in the small particle size range, while the Brown relaxation is the opposite [15].

The viscosity of the fluid medium has no impact on Néel relaxation, but Brown relaxation is proportional to the viscosity coefficient. Therefore, thinning the viscosity of the fluid medium can shorten the relaxation time in a larger size range, but the effect is tiny in a smaller size range. In addition, Néel relaxation has a negative exponential relationship

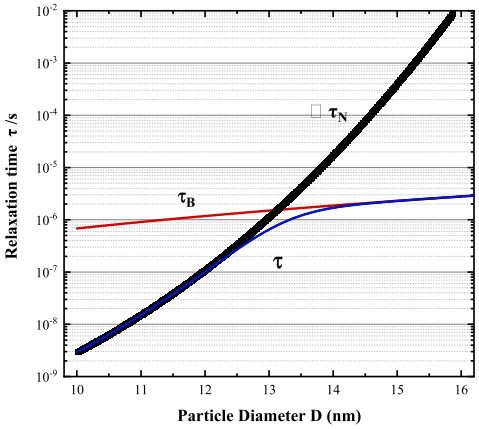

FIGURE 11. Relaxation time of Fe2O3 particles in human blood.

with temperature, while Brown relaxation time is inversely proportional and more sensitive to temperature. Therefore, temperature has a more significant effect on magnetic force in the particle size range dominated by Brown relaxation. In general, the effect of temperature on relaxation and magnetic force is intricate but negligible compared to the influence of MNP particle sizes.

B. MACT-MI SOUND PRESSURE ANALYSIS

According to the magnetic force simulation results, the sound pressure distribution of the model is solved by the sound pressure wave equation. The diameter of the MNPs is 15 nm. The sound pressure distribution on the YOZ plane is shown in Figure 12 and Figure 13.

Due to the characteristics of the dipole sound source, sound pressure extremes appear at the upper and lower boundaries of the model, and the directions are opposite. This is due to the difference in particle concentration inside and outside the boundary.

To obtain the sound pressure distribution of the MNP cluster model, take the line in which the starting point A and the ending point B are (0, 5, 10) and (0, 5, 28), respectively. The results show that the sound pressure peak appears at the boundary of the MNPS cluster, and the distance between peak values is exactly equal to the distance between the upper and lower surfaces of the cylinder cluster model, as shown in Figure 13. In addition, due to the stronger magnetic force near the Maxwell coil, the sound pressure amplitude above the MNP cluster is higher than that below.

1) EFFECT OF FLUID MEDIUM ON SOUND PRESSURE

The sound pressures in fluid media with different temperatures and viscosities are compared while strictly controlling the variables. When D $<$ 13.5 nm, the sound pressure gap between different temperatures and viscosities is weak. Therefore, the data in Figure 13 were obtained when the particle size D = 15 nm. At this particle size, the relaxation time is dominated by Brown relaxation, and both the temperature

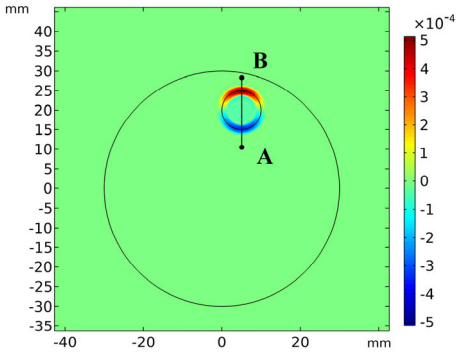

FIGURE 12. t = 0.9μs Sound pressure distribution on the YOZ plane.

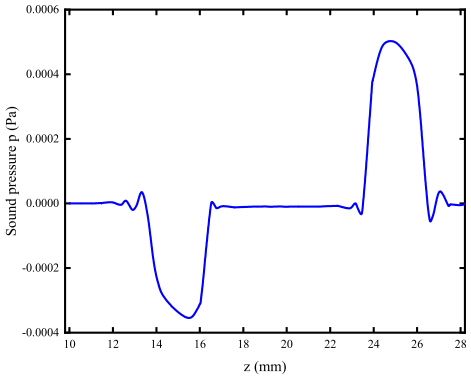

FIGURE 13. t = 0.9μs The sound pressure curve.

and viscosity of the fluid medium affect the sound pressure. In Figure 14 as the temperature increases, the thermal motions of MNPs accelerate, and the amplitude of the sound pressure signal shows an upward trend. However, the sound pressure amplitude in the fluid medium with a smaller viscosity coefficient is higher, which is more conducive to the acquisition of sound signals, as shown in Figure 15.

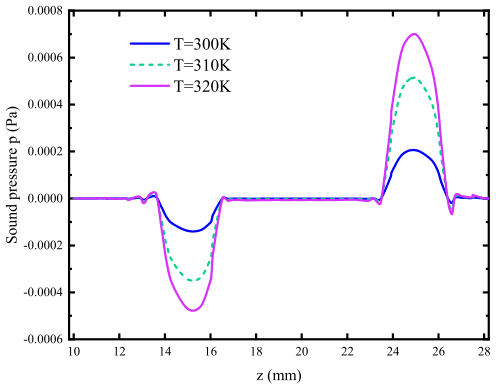

FIGURE 14. The sound pressure curve at different temperatures.

2) EFFECT OF MNP DIAMETER ON SOUND PRESSURE

In the study of magnetic force, the optimal particle size is predicted to be approximately 13.5 nm. Therefore, this paper

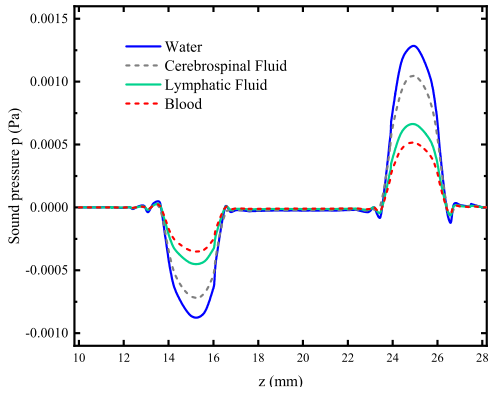

FIGURE 15. T = 310 K, the sound pressure curve at different viscosities.

studies the sound pressure distribution of four kinds of MNPs with particle sizes of 10 nm, 12 nm, 13.5 nm, and 15 nm. The fluid medium is human blood, whose temperature is T = 310 K and viscosity coefficient is 3.65×10^{-3} Pa.s. Figure 16 shows that although the volume of MNPs is the largest when D = 15 nm, the sound pressure amplitude is the weakest compared to other particle sizes. Therefore, larger MNPs cannot generate stronger magneto-acoustic signals. In contrast, MNPs in the range of smaller particle diameters may be more conducive to obtaining magneto-acoustic signals. When other parameters are the same, the sound pressure of D = 13.5 nm is more than 5 times that of D = 15 nm. It can be seen that both magnetic force and sound pressure are exceedingly sensitive to the diameters of MNPs. Once the optimal particle size is selected, it has a significant influence on enhancing the effect of magneto-acoustic imaging.

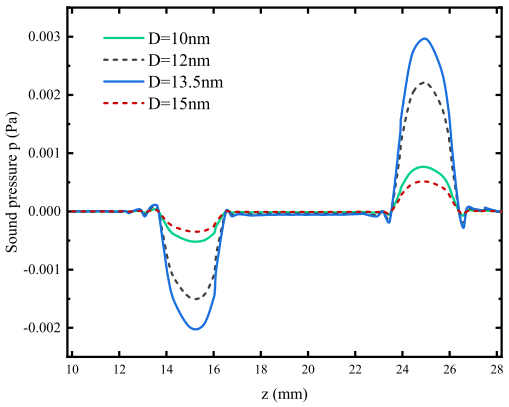

FIGURE 16. Sound pressure curve with different MNP diameters.

Comparing the above three modulation methods, when the diameters of the MNPs are 15 nm, the sound pressure can reach more than 0.003 Pa. However, by adjusting the temperature or viscosity of the fluid medium, the sound pressure amplitude does not exceed 0.0015 Pa. It can be seen that selecting MNPs with the most ideal particle size can greatly improve the magnetic force and sound pressure of MACT-MI by means of the relaxation mechanism. In this way, it reduces the concentration of MNPs in MACT-MI, reduces the metabolic pressure of the kidney, and shows unique advantages in the improvement of imaging effects.

C. EFFECTS OF PARTICLE SIZE DISTRIBUTION ON MAGNETIC FORCE AND SOUND PRESSURE

In the study of the particle size distribution of multi-size particles, the abovementioned initial simulation conditions are still selected. On this basis, it is assumed that the average diameter of the particles is D_0, and the magnetic force and sound pressure of the MNPs are obtained under four distributions of $\sigma = 0.01$, $\sigma = 0.025$, $\sigma = 0.05$, and $\sigma = 0.1$. The calculation results of the magnetic force at the center M(0,5,20) of the MNP cluster are shown in Figure 17. The synthesized magnetic force presents a maximum value at $D_0 = 13.5$ nm, and the magnetic force in the small particle size range is slightly larger than the MNP population, with $D_0 > 13.5$ nm. In addition, when σ is smaller, the particle size distribution of MNPs is more uniform, and the synthesized magnetic force is stronger. When σ rises, the particle size of MNPs becomes disorganized, and the synthetic magnetic force also decreases.

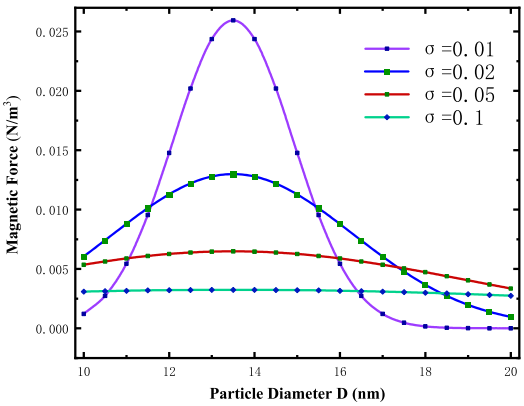

FIGURE 17. t = 0.2μs, synthetic magnetic forces by different particle size distributions.

Furthermore, the effect of sound pressure on the uniformity of the particle size of MNPs was investigated. When $D_0 = 13.5$ nm, the sound pressure on the axis between two points A and B is shown in Figure 18. Similar to the magnetic results, when σ is larger, the number of extremely large or extremely small particles in the particle population increases. The more inhomogeneous the particle size distribution of MNPs is, the more obvious the decrease in the sound pressure of multi-size MNP synthesis.

In MACT-MI, increasing the concentration of MNPs is one of the easiest and most convenient means to enhance the magneto-acoustic signal. However, considering their clinical medical use, the concentration of magnetic nanoparticles should be limited. Otherwise, the concentration of magnetic nanoparticles in the human body is too high, and the degradation is unfavorable, which can burden and even damage the kidneys. Adjusting the magnetic nanoparticle parameters

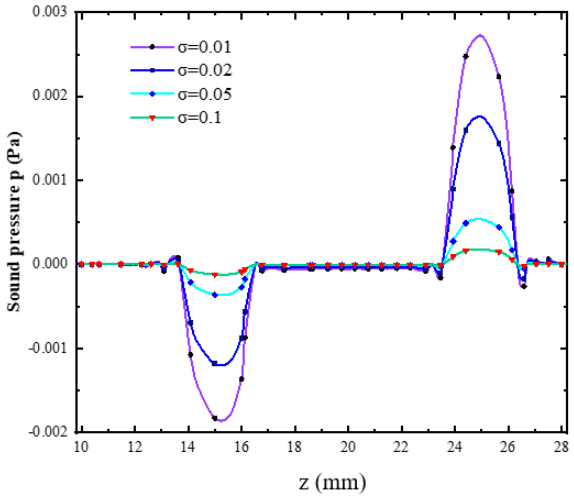

FIGURE 18. t = 0.9μs, synthetic sound pressures for different particle size distributions.

can be used as a means of compensation under the limitation of particle concentration. As seen in Figure 19, with all the remaining parameters being the same, the MNPs with D = 13.5 nm need only one-fourth of the original concentration to achieve a magnetic amplitude close to the initial parameters (D = 15 nm, concentration = 4 mg Fe/ml). When the particle size is slightly dispersed at the optimal size (D = 13.5 nm), the magnetic force also decreases slightly, but it can still be maintained in a more desirable range. This indicates that it is feasible and effective to enhance the signal intensity and reduce the concentration of MNPs by adjusting the particle size.

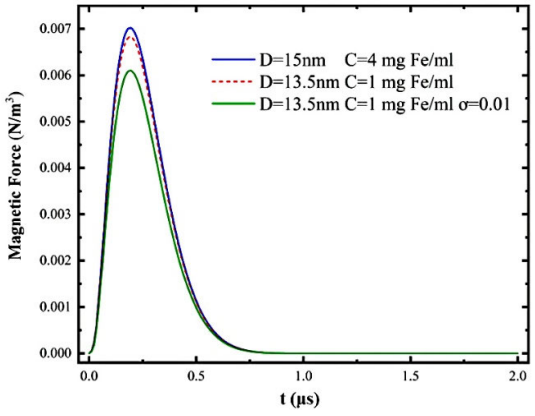

FIGURE 19. Comparison of magnetic force under the combined effect of concentration and particle size.

IV. CONCLUSION

In this paper, through theoretical analysis and numerical simulation, the relaxation and magnetization characteristics of magnetic nanoparticles in a fluid environment are studied. Preliminary explorations were made to optimize MNPs to improve the imaging quality of MACT-MI. In this paper, the magnetic calculation method of MNPs under the relaxation mechanism is specifically studied, and the relationship between the sound pressure signal and the particle size of MNPs and the fluid medium environment is explored. Combining theoretical analysis and simulation results, the following conclusions are drawn:

1) The magnetic susceptibility of MNPs is inversely proportional to their relaxation time in a fluid environment. By shortening the relaxation time, the magnetic susceptibility of MNPs can be increased to a certain extent, thereby elevating the level of the magneto-acoustic signal.

2) With the combinations of particle volume and relaxation time, MACT-MI has an optimal imaging particle diameter. Selecting and using MNPs with the optimal particle size can significantly upgrade the amplitude of magnetic force and sound pressure, which is beneficial to the collection of magneto-acoustic signals. This can reduce the concentration of MNPs to a certain extent and reduce the metabolic pressure on the kidneys.

3) In the range of larger particle sizes, thinning the viscosity and raising the temperature of the fluid medium have positive effects on the magnetic force and sound pressure. In addition, according to the actual clinical temperature (such as heating in hyperthermia and specific cooling methods to reduce the activity of certain biological enzymes) and target tissue, the particle size of MNPs can be selected and controlled within an ideal range so that the actual clinical application of MACT-MI is more targeted and the imaging effect is better.

4) If the particle size distribution in the magnetic nanoparticle population is too non-uniform, the magnetic force and sound pressure will be significantly weakened, which makes the imaging effect unsatisfactory.

This article comprehensively considers the influence of the relaxation time of MNPs on the magnetic susceptibility and studies the effects of the MNPs themselves and the fluid medium environment on MACT-MI, but this study lacks experiments to further research and verify the simulation results. In addition, the surface of the MNP magnetic substance is covered with a magnetic neutral coating to prevent agglomeration. The coating thickness δ may slightly prolong the Brown relaxation time, which needs to be further refined. Furthermore, it should be noted that temperature changes the viscosity of the fluid medium to a certain extent. In conclusion, on the basis of previous research, this article further explores the magnetic sound source mechanism of MACT-MI. This further consolidates the theoretical basis of MACT-MI and provides guidance and a reference for selecting MNPs for superior imaging. It provides prospective exploration ideas for the application of MNPs in the field of biomedical marking.

REFERENCES

[1] S. J. Norton and T. Vo-Dinh, "Imaging the distribution of magnetic nanoparticles with ultrasound," *IEEE Trans. Med. Imag.*, vol. 26, no. 5, pp. 660–666, May 2007.

[2] H. Gang and B. He, "Magnetoacoustic imaging of magnetic iron oxide nanoparticles embedded in biological tissues with microsecond magnetic stimulation," *Appl. Phys. Lett.*, vol. 100, no. 1, pp. 484–488, Jan. 2012.
[3] L. Mariappan, Q. Shao, C. Jiang, K. Yu, S. Ashkenazi, J. C. Bischof, and B. He, "Magneto acoustic tomography with short pulsed magnetic field for *in-vivo* imaging of magnetic iron oxide nanoparticles," *Nanomed., Nanotechnol., Biol. Med.*, vol. 12, no. 3, pp. 689–699, Apr. 2016.
[4] X. H. Yan, Z. Ying, and G. Q. Liu, "Simulation research on effect of magnetic nanoparticles on physical process of magneto-acoustic tomography with magnetic induction," *Chin. Phys. B*, vol. 27, no. 10, pp. 314–322, 2018.
[5] X. Yan, "Simulation research on forward problem of magnetoacoustic concentration tomography of magnetic nanoparticles with magnetic induction in saturation magnetization state," *J. Phys. D, Appl. Phys.*, vol. 54, no. 7, pp. 463–470, Oct. 2020.
[6] X. Yan, "Implementation method for magneto-acoustic concentration tomography with magnetic induction (MACT-MI) based on the method of moments," *Comput. Biol. Med.* vol. 12, vol. no.8, pp. 104–105, 2021.
[7] Y. Xiaoheng, "Simulation of the influence of permanent magnet with same polarity on induction magneto-acoustic magnetic particle concentration imaging process," *Chin. J. Elect. Technol.*, vol. 37, no. 4, pp. 210–218, Feb. 2022.
[8] J. W. M. Bulte, "Superparamagnetic iron oxides as MPI tracers: A primer and review of early applications," *Adv. Drug Del. Rev.*, vol. 138, pp. 293–301, Jan. 2019.
[9] A. Tsalach, I. Steinberg, and I. Gannot, "Tumor localization using magnetic nanoparticle-induced acoustic signals," *IEEE Trans. Biomed. Eng.*, vol. 61, no. 8, pp. 2313–2323, Aug. 2014.
[10] X. Feng, F. Gao, and Y. Zheng, "Modulatable magnetically mediated thermoacoustic imaging with magnetic nanoparticles," *Appl. Phys. Lett.*, vol. 106, no. 15, Apr. 2015, Art. no. 153702.
[11] D. Piao, "Magneto-thermal-acoustic differential-frequency imaging of magnetic nanoparticle with magnetic spatial localization: A theoretical prediction," *Proc. SPIE*, vol. 10066, Feb. 2017, Art. no. 100660F.
[12] X. Feng, G. Fei, and Y. Zheng, "A self-monitored theranostic platform based on nanoparticle hyperthermia therapy and alternating magnetic field induced thermoacoustic imaging," *Proc. SPIE*, vol. 9323, May 2015, Art. no. 93234N-1.
[13] Y. Xu, A. Karmakar, D. Wang, M. W. Mahmood, F. Watanabe, Y. Zhang, A. Fejleh, P. Fejleh, Z. Li, G. Kannarpady, S. Ali, A. R. Biris, and A. S. Biris, "Multifunctional Fe3O4 cored magnetic-quantum dot fluorescent nanocomposites for RF nanohyperthermia of cancer cells," *J. Phys. Chem. C*, vol. 114, no. 11, pp. 5020–5026, Mar. 2010.
[14] R. E. Rosensweig, "Heating magnetic fluid with alternating magnetic field," *J. Magn. Magn. Mater.*, vol. 252, pp. 370–374, Nov. 2002.
[15] E. Romanus, M. Hückel, C. Groß, S. Prass, W. Weitschies, R. Bräuer, and P. Weber, "Magnetic nanoparticle relaxation measurement as a novel tool for *in vivo* diagnostics," *J. Magn. Magn. Mater.*, vol. 252, pp. 387–389, Nov. 2002.
[16] J. P. Fortin, F. Gazeau, and C. Wilhelm, "Intracellular heating of living cells through Néel relaxation of magnetic nanoparticles," *Eur. Biophys. J.*, vol. 37, no. 2, pp. 223–228, 2008.
[17] R. Hergt, S. Dutz, and M. Zeisberger, "Validity limits of the Néel relaxation model of magnetic nanoparticles for hyperthermia," *Nanotechnology*, vol. 21, no. 1, Nov. 2010, Art. no. 015706.
[18] K. Y. Yoon, "Synthesis of iron oxide nanoclusters with enhanced magnetization and their applications in pulsed magneto-motive ultrasound imaging," *Nano*, vol. 10, no. 5, pp. 73–82, May 2015.
[19] I. M. Perreard, D. B. Reeves, X. Zhang, E. Kuehlert, E. R. Forauer, and J. B. Weaver, "Temperature of the magnetic nanoparticle microenvironment: Estimation from relaxation times," *Phys. Med. Biol.*, vol. 59, no. 5, pp. 1109–1119, Mar. 2014.
[20] G. P. Guo, Y. Gao, and Z. Y. Li, "Second harmonic magnetoacoustic responses of magnetic nanoparticles in magnetoacoustic tomography with magnetic induction," *Chin. Phys. B*, vol. 29, no. 3, pp. 236–251, Mar. 2020.
[21] *Magnetic Particle Imaging: An Introduction to Imaging Principles and Scannerinstrumentation*, Springer, New York, NY, USA, 2012, pp. 12–22.
[22] *Solar Cell-Operation Principles, Technology and System Applications*, Universiity of New South Wales, Kensington, NSW, Australia, 1998, pp. 34–35.
[23] R. M. Ferguson, K. R. Minard, and K. M. Krishnan, "Optimization of nanoparticle core size for magnetic particle imaging," *J. Magn. Magn. Mater.*, vol. 321, no. 10, pp. 1548–1551, 2009.
[24] S. Zhang, Z. X. Li, and X. Y. Zhang, "Simulation and experiment of magnetodynamic ultrasound imaging based on time inversion," (in Chinese), *Trans. China Electrotech. Soc.* vol. 34, no. 16, pp. 3303–3309, Aug. 2019.

XIAOHENG YAN was born in Liaoning, China, in 1984. She received the master's and Ph.D. degrees from Liaoning Technical University, in 2008 and 2016, respectively.

She is currently an Associate Professor with Liaoning Technical University. Her research interests include electromagnetic ultrasound detection and imaging and biomedical imaging.

DI SUN was born in Liaoning, China, in 1996. She is currently pursuing the master's degree with Liaoning Technical University. Her research interest includes electromagnetic ultrasound imaging.

ZHENGXING LI was born in Henan, China, in 1997. He is currently pursuing the master's degree with Liaoning Technical University. His research interest includes electromagnetic ultrasound imaging.

WEIHUA CHEN was born in Heilongjiang, China, in 1980. He received the master's and Ph.D. degrees from Liaoning Technical University, in 2006 and 2016, respectively.

He is currently an Associate Professor with Liaoning Technical University. His research interests include electromagnetic ultrasound detection and wireless energy transmission technology.